AIMS Materials Science, 12(2): 301–317.
DOI: 10.3934/matersci.2025016
Received: 03 March 2025
Revised: 04 April 2025
Accepted: 14 April 2025
Published: 17 April 2025

http://www.aimspress.com/journal/Materials

Research article

A photothermal soft actuator based on graphene/PDMS composite materials reinforced by carbon fiber skeleton

Jincong Chen[1,2,3], Xiaodong Zhao[1,2,3] and Haiyan Zhao[1,2,3,*]

[1] Department of Mechanical Engineering, Tsinghua University, Beijing 100084, PR China
[2] State Key Laboratory of Tribology in Advanced Equipment, Tsinghua University, Beijing 100084, PR China
[3] State Key Laboratory of Clean and Efficient Turbomachinery Power Equipment, Department of Mechanical Engineering, Tsinghua University, Beijing, 100084, PR China

* **Correspondence:** Email: hyzhao@tsinghua.edu.cn; Tel: +86-10-6278-4578; Fax: +86-10-6278-4578.

Abstract: Soft actuators have garnered significant attention due to their promising applications in wearable devices, soft robotics, and other related fields. However, achieving substantial reversible deformation and high output force simultaneously remains a long-standing challenge. In this study, graphene/polydimethylsiloxane (PDMS) composite materials with high photothermal conversion efficiency and rapid photo-responsiveness were successfully developed. Inspired by the structure of biological muscles and skeletons, a novel approach involving carbon fiber bundles as reinforcement skeletons was proposed to enhance actuator performance. A composite material/carbon fiber skeleton/PDMS actuator was fabricated. With the integration of the carbon fiber skeleton, the actuator demonstrated a remarkable bending angle of 90° (3.5 times greater than that of actuators without the carbon fiber skeleton) and an output force of 0.89 mN (1.34 times higher than that of actuators without the carbon fiber skeleton) under infrared laser irradiation at 4.15 W/cm^2. This advanced actuator holds great potential for applications in areas such as soft robotic grippers and artificial muscles that demand high load-bearing capacity.

Keywords: soft actuator; graphene; carbon fiber; composite; photothermal

1. Introduction

Soft actuators [1,2], capable of responding to external stimuli such as electricity [3,4], light [5,6], temperature [7,8], humidity [9,10], and magnetic fields [11,12], have garnered significant attention due to their versatile applications. They show immense potential in fields like biomimetic robotics [13,14], artificial muscles [15,16], sensors [17,18], and wearable devices [19–21]. Electrical stimulation offers fast response times and high control accuracy, but it requires materials with good conductivity and is susceptible to environmental factors and deformation [22]. Additionally, it necessitates a stable power supply, which complicates circuit design and creates challenges regarding the relationship between connections and deformation, thus limiting its potential applications. Humidity stimulation, on the other hand, is environmentally friendly and energy-efficient, but its slow response time, difficulty in control, and high environmental requirements make it unsuitable for extremely dry or humid conditions [23]. Magnetic field stimulation has the advantages of high safety, low energy consumption, and non-contact control. However, it faces challenges such as a limited control range, restricted material choices, a complex system, and vulnerability to interference from other electronic devices [11]. Among these stimuli, light stands out as a particularly appealing control tool for intelligent robots because it is clean, safe, and efficient and can operate without direct contact with actuators. The non-contact nature of light control enables its application in more intricate and complex environments. More broadly, light stimulation holds considerable promise in the realms of material preparation, device processing, and the regulation of smart devices [24,25]. Therefore, it is crucial to give increased attention to the advancement of smart devices that leverage light stimulation. Thus, based on the photothermal effect to induce expansion/contraction or phase transitions, various smart photothermal responsive actuators have been developed [26,27], such as intelligent biomimetic robots, smart curtains, wearable devices, and so on. These actuators exhibit unique advantages, including high controllability, rapid response, excellent repeatability, superior stability, and high spatial and temporal precision. However, the development of high-performance actuators capable of simultaneously achieving fast responses, large deformations, and high output forces remains a significant challenge.

The primary materials used to develop intelligent soft robots include hydrogels [28,29], shape memory polymers [30,31], two-dimensional transition metal carbides/nitrides [14,32], and carbon materials such as graphene [7,33,34], its derivatives [35,36], and carbon nanotubes [37,38]. Among these, carbon materials are particularly remarkable for their exceptional light absorption and photothermal conversion properties [39]. Within the category of carbon materials, graphene stands out due to its broad light absorption range, high mechanical strength, flexibility, and ease of processing, making it an excellent candidate for photothermal-responsive actuators. In composite materials, the properties of polymer matrices fundamentally determine the characteristics of the overall composite. Typically, carbon materials are combined with polymers that have different thermal expansion coefficients (e.g., polyimide (PI), polypropylene (PP), and polydimethylsiloxane (PDMS)) to form composite films. For instance, Wang et al. [40] developed a three-layer composite soft robot consisting of carbon nanotubes, PDMS, and polyvinylidene fluoride (PVDF), which exhibited rapid responses to liquid, vapor, and light stimuli. Similarly, Hiran Chathuranga et al. [41] introduced a graphene oxide/Fe_3O_4/starch composite soft robot capable of responding quickly to changes in humidity, magnetic fields, and ultraviolet radiation. Among these polymers, PDMS is an elastic material widely used as a matrix for graphene composites due to its excellent optical transparency, flexibility, biocompatibility, stability, and processability [42]. With its high thermal expansion coefficient (3.2×10^{-4} W/K), PDMS enables

the fabrication of actuators with significant deformability. However, due to the intrinsic limitations of PDMS in flexibility, such actuators face challenges in terms of robustness and adaptability to shape changes. Thus, further research is required to enhance their output force.

In this study, inspired by the relationship between animal skeletons and muscles, we propose a novel strategy to enhance the performance of composite actuators by introducing parallel carbon fiber skeletons. Graphene/PDMS composite materials with high photothermal conversion efficiency and rapid photo-responsiveness were successfully fabricated. Leveraging the unique characteristics of these composite materials, a composite material/carbon fiber skeleton/PDMS actuator was designed, wherein the parallel carbon fibers act as the "skeleton", while the composite material layer and the PDMS layer function as the "muscle" wrapped around the carbon fiber skeleton. The resulting actuator achieved an impressive bending angle of 90° (3.5 times greater than that of actuators without the carbon fiber skeleton) and an output force of 0.89 mN (1.34 times greater than that of actuators without the carbon fiber skeleton). The reinforcement mechanism of the carbon fiber skeleton in enhancing actuator performance was systematically investigated through experiments. The applications of biomimetic artificial muscles, mechanical grippers, and biomimetic palms have been realized. This innovative actuator holds significant potential for applications in fields such as soft robotic grippers and artificial muscles requiring high load-bearing capabilities.

2. Materials and methods

2.1. Materials

In this study, graphene with a selected diameter of approximately 15 μm was purchased from Shenzhen Guosen Pilot Technology Co., Ltd. (China). Carbon fiber (filament bundles, density: 1.8 g/cm^3; single fiber diameter: 6.9 μm) was purchased from Toray Co., Ltd. (Japan). The PDMS used in this research was Sylgard 184 silicone elastomer, supplied by Dow Corning (USA). Additionally, N-hexane was obtained from Shanghai Titan Technology Co., Ltd. (China), while acetone was acquired from Modern East Technology Development Co., Ltd. (China) for experimental purposes.

2.2. Preparation of graphene/PDMS composite and thin-film actuators

Initially, the PDMS substrate layer is prepared by mixing the PDMS base solution and curing agent in a beaker at a 10:1 ratio. The mixture is applied onto a glass substrate, placed in a vacuum drying oven, and cured at 100 ℃ for 2 h. Due to the excessive thickness and roughness of commercial carbon fibers, dispersion is required. To achieve this, carbon fiber bundles of a specific length are immersed in acetone and ultrasonically cleaned to remove surface insulation materials and facilitate fiber dispersion. The dispersed carbon fibers are then bundled into groups of 60 single fibers and arranged at fixed intervals (3 mm) on the PDMS substrate to form a carbon fiber skeleton. The optical image of the carbon fiber skeleton laid on the PDMS layer is shown in Figure S1 of the Supporting Information.

Subsequently, the graphene/PDMS composite material is prepared, as illustrated in Figure 1. The preparation begins by mixing PDMS base liquid and curing agent in a beaker at a 10:1 ratio. Graphene is then incorporated into the mixture at a predetermined mass ratio, followed by the addition of n-hexane. The resulting mixture is preliminarily stirred using a magnetic stirrer. Considering the

boiling point of n-hexane (69 ℃), the mixture undergoes ultrasonic mixing at the same temperature to ensure uniformity. Once most of the n-hexane has evaporated, the mixture is applied onto a clean glass substrate and solidified in a vacuum-drying oven to produce a uniform graphene/PDMS composite.

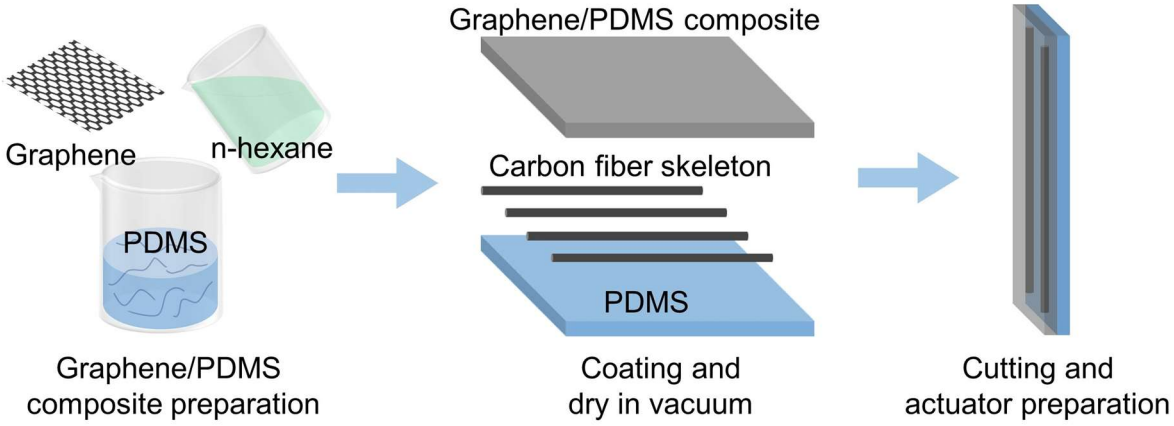

Figure 1. Preparation process of graphene/PDMS composite material and carbon fiber reinforced soft actuator.

For the fabrication of thin-film actuators, the uncured graphene/PDMS composite material is applied over the PDMS substrate and carbon fiber skeleton to create a composite structure comprising the graphene/PDMS layer, carbon fiber skeleton, and PDMS substrate. This structure is placed in a vacuum drying oven and heated at 80 ℃ for 6 h to complete the curing process. After curing, the structure is cut into thin-film actuators with dimensions of 6 × 30 mm^2. Both the composite material layer and PDMS layer have a thickness of approximately 100 μm.

2.3. Characterization and measurement details

The apparent structure and morphology of the composites and actuator were analyzed using a Zeiss high-resolution field emission scanning electron microscope (SEM) and an OLYMPUS BX46 microscope. Raman spectra were acquired using a HORIBA Raman microscope with an excitation wavelength of 532 nm. The manipulated actuator was actuated by a point laser with a wavelength of 808 nm, provided by Radiant Optoelectronics Technology Co., Ltd., Changchun, China. The laser's power density was calibrated with a TP100 optical power meter at a distance of 12 cm. The surface temperature distribution and maximum temperature of the composites were measured and recorded using JENOPTIK IR-TCM HD Infrared Cameras. The actuator's output force was measured using the BSA124S-CW precision electronic balance from Sartorius Scientific Instruments Co., Ltd., while the actuator's bending degree was recorded with the high-definition camera of a mobile phone.

A dedicated system was developed to characterize the output force of the actuators, as shown in Figure 2. The magnitude of the force was measured using a precision balance. The actuator was positioned parallel to the balance, with one end fixed and the other end resting on the balance surface due to gravity. When irradiated by a near-infrared laser, the actuator bent towards the balance, exerting pressure and causing a measurable change in the balance reading. The force output during deformation was characterized by recording the balance readings before and after irradiation. The distance between the laser outlet and the actuator surface was maintained at 12 cm, while the fixed platform was

positioned 3 mm above the balance. For comparison, actuators without a carbon fiber skeleton were fabricated using the same method.

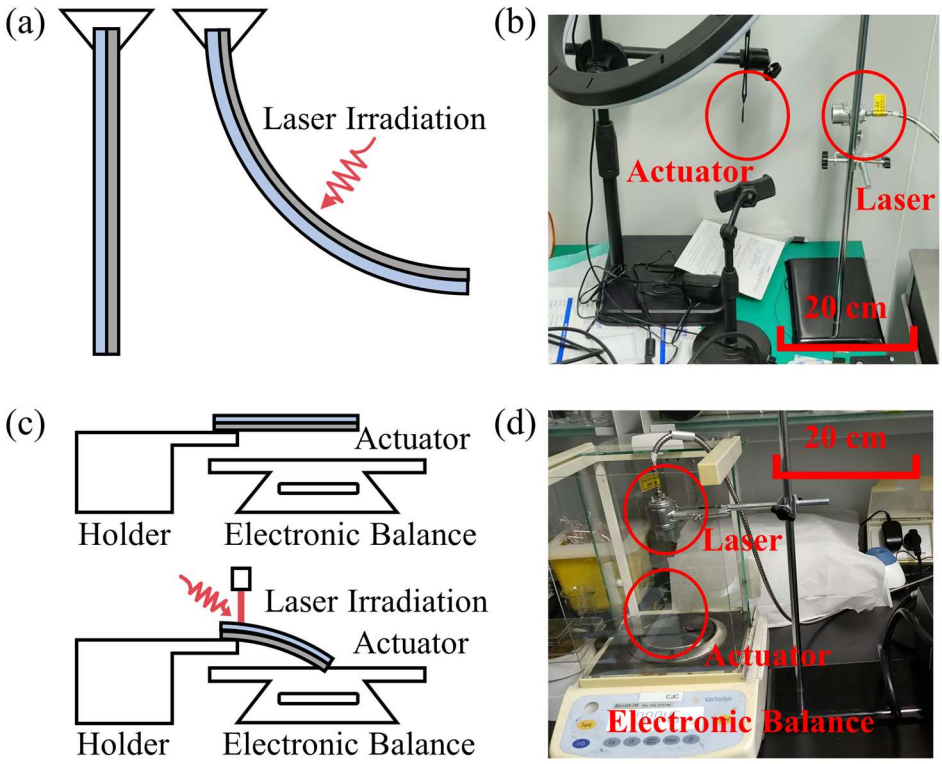

Figure 2. Bending angle and output force detection system. (a) Schematic diagram of the bending performance testing device for soft actuators. (b) Optical image of the bending performance testing device for soft actuators (scale bar: 20 cm). (c) Schematic diagram of the testing device for the output force of soft actuators. (d) Optical image of the testing device for the output force of soft actuators (scale bar: 20 cm).

3. Results and discussion

3.1. Preparation and characterization of graphene/PDMS composite

Figure 1 illustrates a schematic diagram of the preparation process for graphene/PDMS composite materials. The process begins by mixing the PDMS base solution and curing agent in a beaker at a ratio of 10:1. Graphene and an appropriate amount of n-hexane are then added to the uncured PDMS according to a predetermined mass fraction. The mixture is preliminarily stirred using a magnetic stirrer and further subjected to ultrasonic treatment at 69 ℃ to ensure the uniform dispersion of graphene in PDMS and to evaporate the n-hexane. The resulting homogeneous mixture is coated onto a substrate and placed in a vacuum drying oven, where it is cured by heating at 80 ℃ for 6 h. In the preparation of composite materials, graphene tends to cluster and is difficult to disperse, especially in high-viscosity PDMS [43]. Various methods have been developed to enhance graphene dispersion in PDMS, with ultrasonic treatment [44] and the addition of organic solvents [45] being among the most commonly used techniques. In this study, a combination of n-hexane addition and ultrasonic treatment

was utilized to improve dispersion efficiency. Compared with other organic solvents, such as methoxypropanol, isopropanol, ethanol, and ethyl acetate, n-hexane offers unique advantages due to its ultra-high volatility and low boiling point (69 ℃). N-hexane plays a crucial role in several stages of the preparation process. It functions as a diluent, reducing the viscosity of PDMS and delaying its curing time, which enhances the effectiveness of stirring and ultrasonic treatment. During ultrasonic treatment, the constant boiling of n-hexane promotes continuous flow within the mixture, aiding in the dispersion and uniform mixing of graphene and PDMS. Additionally, a small amount of residual n-hexane remains in the composite material during the coating process, making it easier to achieve a smooth application onto the substrate. During the curing stage, the remaining n-hexane volatilizes and helps dissipate heat, which facilitates curing, reduces the likelihood of pores and cracks, and results in high-quality composite materials with smoother surfaces. These properties make n-hexane an indispensable component in the preparation of graphene/PDMS composite materials, ensuring effective processing and superior material performance.

The characterization of the graphene/PDMS composite material layer is presented in Figure 3. Figure 3a shows the optical image of the composite material. The Raman spectrum in Figure 3b confirms that graphene and PDMS are physically mixed uniformly within the composite material, with no evidence of chemical reactions altering their inherent chemical properties. The absorption spectrum of the composite material, shown in Figure 3c, demonstrates an ultra-high light absorption rate of approximately 99%, rendering the material nearly opaque and indicating its strong photothermal conversion capabilities. SEM images in Figure 3d–f provide detailed insights into the shape, size, and distribution of graphene within the composite. Figure 3d shows that graphene nanosheets used in the composite materials are approximately 20 μm in length, exhibiting thin, irregular shapes with uneven edges. Within the composite, PDMS appears gel-like, with smooth, radial edges that act as connectors between various parts. As shown in Figure 3e, when the graphene mass fraction is 5%, PDMS is observed to wrap around the graphene layers, with graphene sheets sparsely embedded. This arrangement contributes to the uniform distribution of graphene, a key factor in ensuring material stability. However, this configuration increases the material's density while limiting the formation of interconnected graphene networks. In contrast, at a 20% graphene mass fraction, minimal PDMS adheres to the graphene layers, facilitating the formation of effective graphene networks. Nonetheless, achieving stable and dense composite films becomes challenging at higher graphene concentrations. The SEM image in Figure 3f displays cross-sections of the composite material and PDMS layers, revealing thicknesses of approximately 84 and 104 μm, respectively. These thicknesses can be adjusted by modifying the coating parameters, and subsequent experiments will use samples with a uniform thickness of approximately 100 μm to maintain consistency. To further investigate the photoresponsiveness and photothermal conversion performance of the composite material, infrared laser irradiation experiments were conducted, with results presented in Figure 3g–i. For these tests, composite samples were cut into 10 × 10 mm square blocks and irradiated at their centers using an infrared laser positioned 12 cm from the sample surface, corresponding to the operating distance in actuation processes. The laser power density at this distance was calibrated using a power meter. Figure 3g illustrates the temperature evolution of composite materials with varying graphene concentrations under laser irradiation at a power density of 2.77 W/cm^2. The results indicate that the surface temperature increases with longer exposure times and higher graphene concentrations. Greater graphene concentrations lead to higher initial heating rates, temperature gradients, and maximum temperatures, reflecting improved photothermal conversion efficiency due to greater graphene

involvement. Figure 3h highlights the temperature changes of the composite material with a 5% graphene mass fraction under different power densities of infrared light. Over time, the surface temperature stabilizes as graphene's excellent thermal conductivity ensures uniform heat distribution. At a high power density of 4.15 W/cm^2, the surface temperature of the composite material approaches 130 °C, demonstrating its rapid light responsiveness and efficient photothermal conversion. Figure 3i tracks the temperature evolution of the composite material over eight cycles of infrared laser irradiation at 2.77 W/cm^2 followed by air cooling. Consistent temperature-time curves across all cycles emphasize the material's excellent repeatability in photothermal conversion.

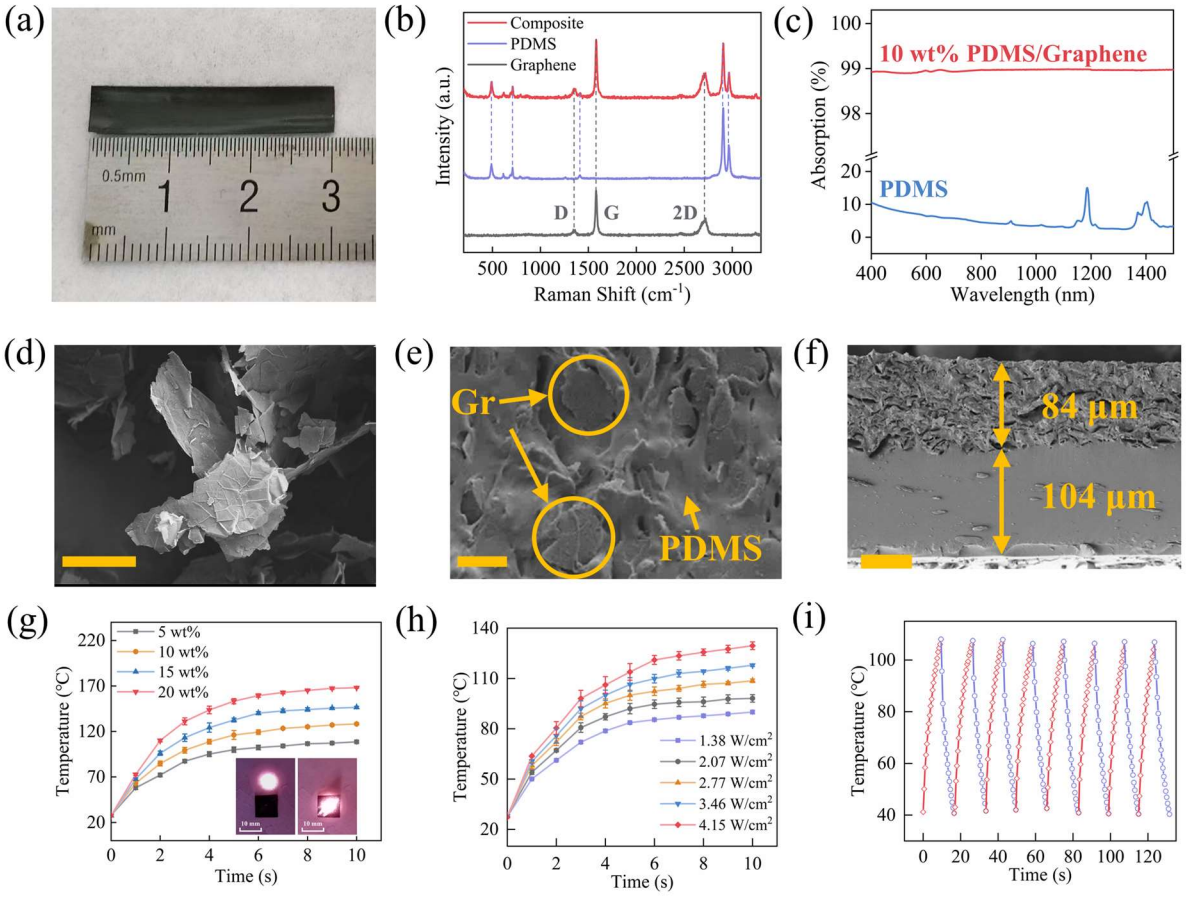

Figure 3. Characterization of the graphene/PDMS composite. (a) Optical image of graphene/PDMS composite. (b) Raman spectra of the graphene, PDMS film, and graphene/PDMS composite. (c) Absorption spectra of PDMS, graphene/PDMS composite with 10 wt% graphene. (d) SEM image of graphene (scale bar: 5 μm). (e) SEM image of graphene/PDMS composite at 5% graphene mass fraction (scale bar: 10 μm). (f) Cross-sectional SEM image of a bilayer film consisting of a graphene/PDMS composite layer and a pure PDMS layer (scale bar: 50 μm). (g) Temperature and time dependence of graphene/PDMS composite materials with different graphene mass ratios irradiated by a 2.77 W/cm^2 infrared laser. (h) Temperature and time dependence of graphene/PDMS composite materials with 5 wt% graphene irradiated by infrared laser with different power densities. (i) Photothermal performances of graphene/PDMS composite materials irradiated by a 2.77 W/cm^2 infrared laser for 8 cycles.

Based on the graphene/PDMS composite material's exceptional photoresponsiveness and photothermal conversion performance, a double-layer optically driven thermal expansion actuator can be constructed by combining the composite material layer with a PDMS layer. However, the inherent softness of PDMS restricts the actuator's ability to support large loads or achieve significant deformation angles. To address these limitations, this study incorporates carbon fiber to enhance actuation performance. Although graphene with a high mass fraction can bring higher temperatures, it greatly weakens the mechanical properties of composite materials, making it difficult to wrap carbon fibers well and achieve the goal of simultaneously increasing the bending angle and output force. Therefore, in the following, a soft actuator is fabricated using a composite material with a 5 wt% graphene mass fraction to evaluate the reinforcing effect and underlying mechanism of carbon fiber.

3.2. The influence of a carbon fiber skeleton on composite soft actuators

To enhance the actuation performance of soft actuators, carbon fiber is employed as a reinforcing filler in this study. Inspired by the structural relationship between biological skeletons and muscles, graphene/PDMS composite materials and PDMS layers are considered as the "muscles", while parallel carbon fiber arrays act as the "biological skeleton". The schematic diagram of the actuator preparation process is shown in Figure 1. The carbon fiber skeleton is positioned between the graphene/PDMS composite material and the PDMS layer. The preparation process begins with the fabrication of a PDMS substrate layer. Carbon fibers are immersed in acetone and subjected to ultrasonic dispersion treatment for 30 min. Bundles of 60 carbon fibers are then arranged at fixed intervals of 3 mm on the PDMS substrate to form the carbon fiber skeleton. Uncured graphene/PDMS composite material is subsequently layered onto the PDMS substrate and carbon fiber skeleton. The PDMS and composite material layers encapsulate the carbon fibers, forming a composite structure of composite material/carbon fiber/PDMS. The structure is placed in a vacuum drying oven and cured at 80 ℃ for 6 h. The lower curing temperature and extended curing time ensure complete evaporation of n-hexane. Finally, the composite structure is cut into thin-film actuators measuring 6 × 30 mm^2, with the composite material and PDMS layers both having a thickness of approximately 100 μm.

In this study, carbon fibers are incorporated into the actuator in various forms—powder, short bundle, interlayer, and bundle—to evaluate the effects of different configurations, as illustrated in Figure 4. When carbon fibers are used in powder form, the preparation process is similar to that of graphene/PDMS composite materials. Carbon fiber powder/PDMS composites are prepared by diluting with n-hexane and dispersing with ultrasonic treatment. The carbon fiber powder used, with a 50-mesh specification, is supplied by Toray, Japan. The resulting actuator consists of two layers: a carbon fiber powder/PDMS composite material layer and a pure PDMS layer, as shown in Figure 4a. This method produces relatively uniform composite materials and actuators. When carbon fibers are introduced in short bundles, the preparation process also follows that of graphene/PDMS composites. Short bundle carbon fibers, with an average length of approximately 2 mm, are obtained by cutting. However, this method results in uneven dispersion of the carbon fibers within the PDMS, preventing the formation of a uniform composite material, as shown in Figure 4b. Therefore, short bundles are not suitable for fabricating composite materials and actuators. In the interlayer configuration, a carbon fiber sheet is placed between the graphene/PDMS composite material layer and the PDMS layer, forming a three-layer actuator structure, as shown in Figure 4c. However, poor bonding between the upper and lower composite layers, the PDMS layer, and the carbon fiber layer causes detachment

issues, making this method unsuitable for preparing actuators. When carbon fibers are used in the form of bundles, they are laid on the PDMS substrate at fixed intervals and specific quantities, as shown in Figure 4d. Initially, carbon fibers are dispersed by soaking in acetone and undergoing ultrasonic treatment. Bundles of uniform size are formed by weighing approximately 60 carbon fibers using a precision electronic balance. These bundles are then arranged parallel to the PDMS layer surface, with a spacing of 3 mm, and covered with the graphene/PDMS composite material. Due to the strong bonding between the composite material and the PDMS layer, this method produces a uniform and dense bilayer actuator. Among the configurations tested, the carbon fiber morphologies in Figure 4a,d form uniform double-layer composite structures. Therefore, it is necessary to compare the actuation performance of these configurations to determine the most suitable preparation method.

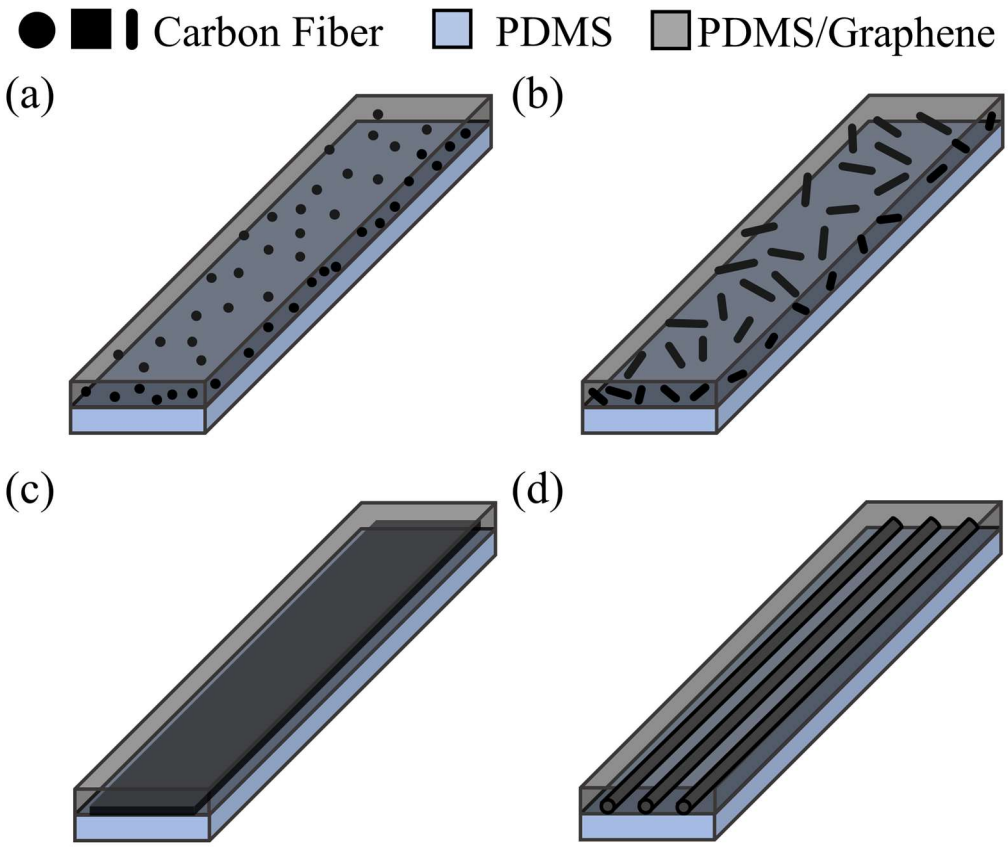

Figure 4. Schematic diagrams of actuators prepared based on different carbon fiber morphologies. (a) Carbon fiber powder. (b) Carbon fiber short bundle. (c) Carbon fiber layer. (d) Carbon fiber bundles.

Here, we compare the effects of different carbon fiber morphologies on the actuation performance of soft actuators. The actuation performance tests primarily evaluate the response speed, motion amplitude, periodic stability, and output force of the actuators. The actuators tested measure 30 mm in length and 6 mm in width. Leveraging the excellent photoresponsiveness and photothermal conversion properties of graphene/PDMS composite materials, the actuators are driven by infrared laser irradiation with a wavelength of 808 nm. The laser outlet is positioned approximately 12 cm from the actuator surface, producing a laser spot with a diameter of about 8.5 mm. Each actuator is fixed on a bracket,

and the position of the laser outlet is adjusted to ensure the laser targets the middle of the actuator during each test.

Due to the photothermal conversion capability of the composite materials, the soft actuators undergo thermal expansion upon laser irradiation. Since the thermal expansion of the PDMS layer is greater than that of the composite material layer, the actuator bends toward the composite material layer, as illustrated in Figure 2a. To assess the bending amplitude and bending speed, a testing device, shown in Figure 2b, is employed. In addition to motion amplitude, another critical indicator of actuation performance is the load capacity. While many related studies measure mechanical properties such as elastic modulus and tensile strength to evaluate material reinforcement, we employ an electronic balance to determine the output force of the soft actuator. This approach provides a direct characterization of the load capacity and material enhancement. The schematic diagram of the measuring device is shown in Figure 2c, and its optical image is displayed in Figure 2d. One end of the soft actuator is fixed to the bracket, while the other end is suspended above the electronic balance, with a height difference of 3 mm between the bracket and the balance. Upon infrared laser stimulation, the actuator bends and exerts pressure on the tray of the electronic balance. The magnitude of the output force is calculated from the readings of the electronic balance.

The actuation performance of the actuators measured using these two devices is shown in Figure 5. Figure 5a compares the bending angles of actuators without carbon fiber and those containing carbon fiber powder and carbon fiber bundles under different power densities. In the figure, “60” and “120” represent carbon fiber bundles composed of 60 and 120 carbon fibers, respectively. As shown in Figure 5a, the carbon fiber skeleton significantly enhances the bending amplitude. The carbon fiber skeleton (60) increases the bending angle from 20° to approximately 90°, while the carbon fiber skeleton (120) increases it to about 55°. The reinforcement effect of the carbon fiber skeleton (60) is stronger than that of the carbon fiber skeleton (120). Figure 5b illustrates the bending and recovery speeds of actuators without carbon fiber and those with carbon fiber powder and carbon fiber bundles under the same power density (4.15 W/cm^2). The results indicate that the carbon fiber skeleton substantially improves both bending and recovery speeds, with the carbon fiber skeleton (60) exhibiting faster speeds than the carbon fiber skeleton (120). Figure 5c presents the output force of different actuators at various laser power densities. At low power densities, actuators reinforced with carbon fiber skeletons exhibit nearly negligible output force, similar to those without carbon fiber. However, at high power densities, the output force of actuators with carbon fiber skeletons surpasses those without. Additionally, the output force of the carbon fiber skeleton (120) exceeds that of the carbon fiber skeleton (60). At 4.15 W/cm^2, the output force of the carbon fiber skeleton (120) reaches 0.89 mN, while that of the carbon fiber skeleton (60) reaches 0.79 mN, representing increases of 2.34 and 2.08 times, respectively, compared to actuators without carbon fiber. Figure 5d shows the angle variation of the actuator with the carbon fiber skeleton (60) over 100 driving cycles, demonstrating its excellent stability. To investigate the reinforcement mechanism of the carbon fiber skeleton, we compared the actuation performance of actuators with the carbon fiber skeleton (60) placed in different layers—either on the PDMS layer or the composite material layer. The results, shown in Figure 5e,f, indicate that when the carbon fiber skeleton is located in the composite material layer, the actuator achieves a larger bending angle and faster bending speed than when it is in the PDMS layer. These findings demonstrate that the actuator performs better when carbon fiber bundles are used as the skeleton.

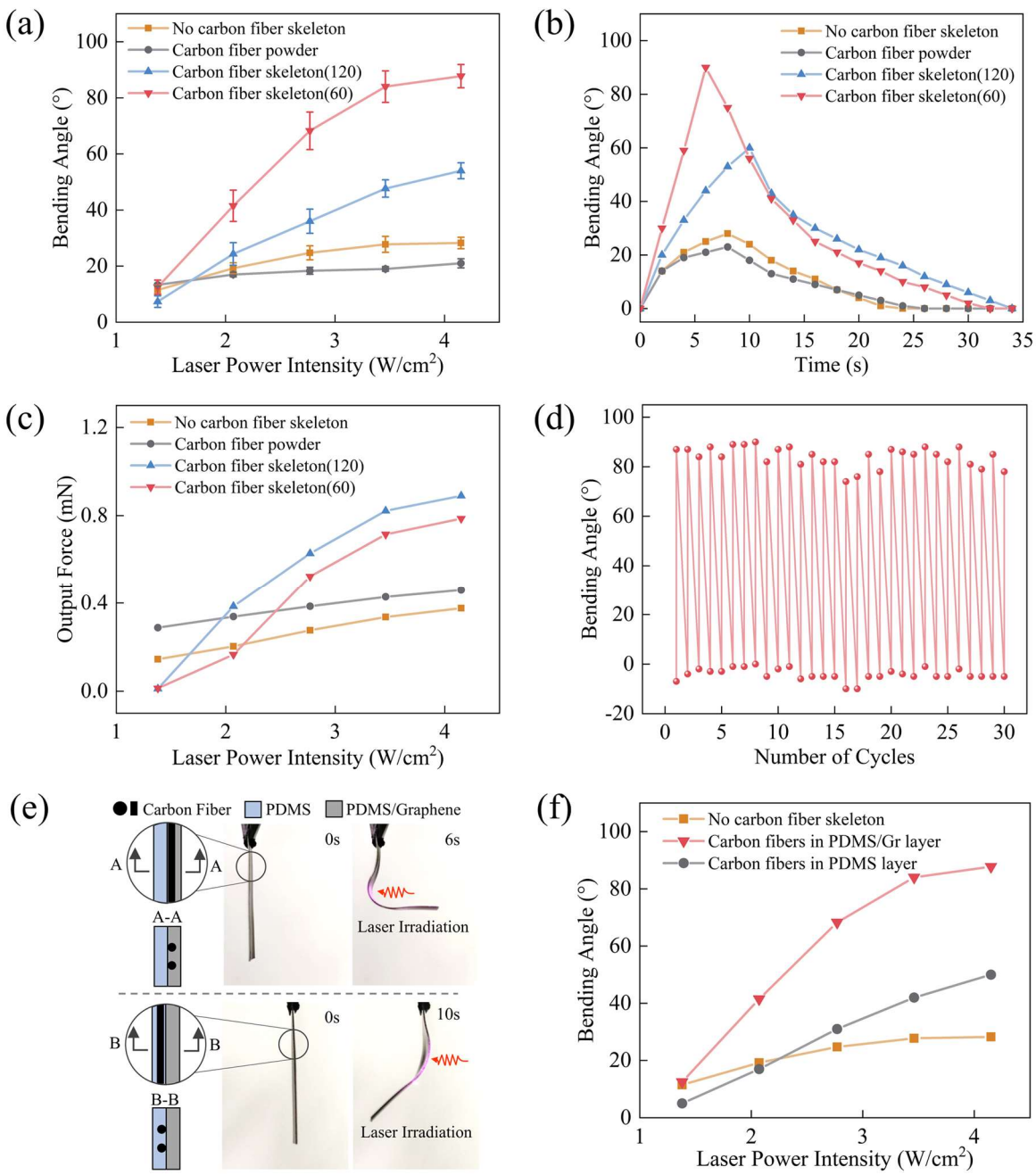

Figure 5. The actuation performance of the actuator. (a) Bending angles at different laser power densities. (b) The relationship between bending angle and time. (c) Output force at different laser power densities. (d) 100 cycles of bending performance. (e) Schematic diagram of carbon fiber in different layers and optical image of actuator bending. (f) The bending angle of the actuator under different laser powers when the carbon fiber is in different layers.

Based on these observations, the reinforcement mechanism of carbon fiber-reinforced soft actuators is analyzed. The impact of carbon fiber on actuation performance is primarily reflected in two aspects. First, carbon fiber limits the deformation of the layer in which it is embedded. Due to its very low thermal expansion coefficient, carbon fiber tightly bonds with the surrounding layer,

constraining its thermal expansion. This limitation creates a significant difference in thermal expansion between the two layers, resulting in a larger bending angle. Consequently, the actuator bends toward the side containing the carbon fiber skeleton. Second, the carbon fiber skeleton increases the stiffness of the actuator, providing greater resistance to deformation. This increased stiffness explains why actuators with carbon fiber skeletons produce smaller output forces at low power densities than those without carbon fiber. However, greater stiffness also enhances the actuator's load capacity, enabling it to resist deformation more effectively. This relationship accounts for the higher output force of the carbon fiber skeleton (120) compared to the carbon fiber skeleton (60), despite the smaller bending angle. We develop an orthogonal anisotropy model to calculate the elastic modulus and thermal expansion coefficient of composite materials with varying carbon fiber contents, as presented in Table S1 of the Supporting Information. It can be observed that the carbon fiber content significantly affects the elastic modulus and thermal expansion coefficient along the direction of the carbon fiber skeleton, with limited impacts in other directions. The deformation of actuators with different carbon fiber contents is calculated using finite element models, and the results are shown in Figure S2. These results are found to be in good agreement with the experimental data, further confirming the mechanism of carbon fiber-reinforced actuators.

Based on the excellent bending and output capabilities, actuators can be applied to a wide range of biomimetic intelligent robot applications. In this study, we demonstrate the use of the actuator in biomimetic artificial muscles, as illustrated in Figure 6. Figure 6 presents optical images of the actuator mimicking the movement of the biceps and lifting a heavy object. The actuator in Figure 6a includes carbon fiber skeletons, whereas the actuator in Figure 6b does not, serving as a comparison. The weight of the object in the images is 0.082 g, while the actuator weighs approximately 0.048 g. It can be observed that the actuator containing carbon fiber skeletons is capable of lifting objects up to 1.7 times its own weight, while the actuator without carbon fiber skeletons struggles to cause any displacement. This clearly highlights the potential for future applications of our actuators.

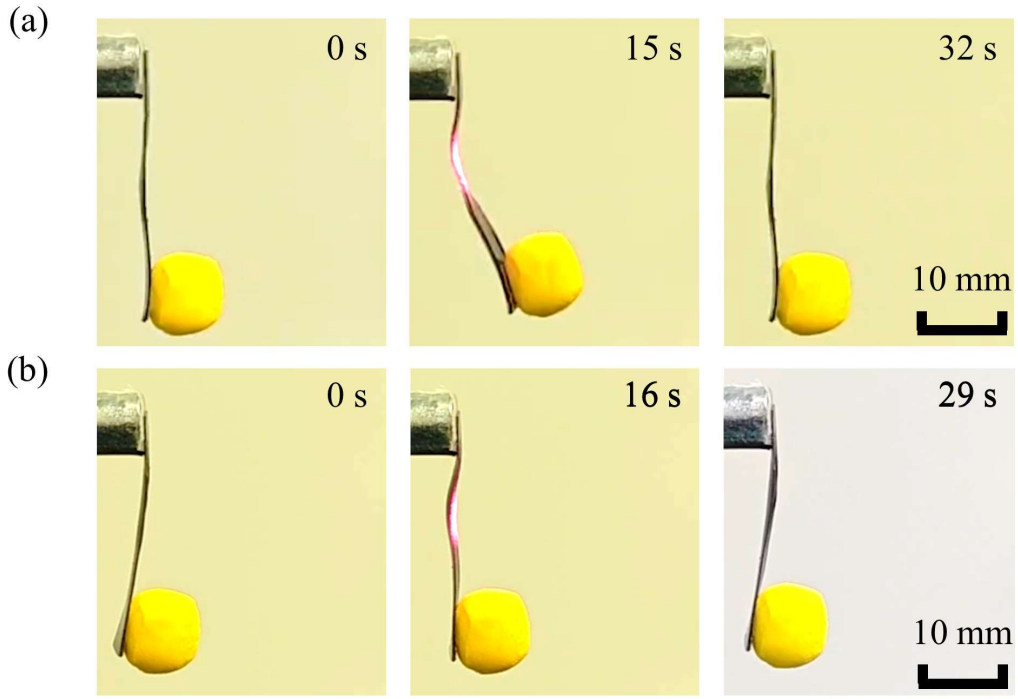

Figure 6. Application of biomimetic artificial muscles. (a) Optical images of artificial muscle with carbon fiber skeleton bicep curl flexion over time. (b) Optical images of artificial muscle without carbon fiber skeleton bicep curl flexion over time.

4. Conclusions

In summary, a graphene/PDMS composite material with high photothermal conversion efficiency and rapid photoresponse has been successfully prepared. Building on this, a composite material/carbon fiber skeleton/PDMS soft actuator was developed. The effects of different forms of carbon fiber—powder, short bundle, interlayer, and bundle—on actuator performance were compared, and carbon fiber bundles were identified as the most suitable reinforcement form. Accordingly, a new strategy for enhancing soft actuators using a carbon fiber skeleton is proposed. The carbon fiber skeleton actuator demonstrates a large reversible bending capability and improved output force. The carbon fiber skeleton serves two critical roles. First, it reduces the thermal expansion coefficient along the direction of the carbon fiber skeleton, significantly increasing the bending angle. Second, it enhances the actuator's stiffness, providing structural support akin to a biological skeleton. This increased stiffness boosts the actuator's resistance to deformation, thereby improving its output force and facilitating the recovery of bending deformation. Under laser irradiation at a power density of 4.15 W/cm^2, the carbon fiber-reinforced actuator achieves a maximum bending angle of 90° (3.5 times greater than that of an actuator without added carbon fiber) and an output force of 0.89 mN (1.34 times higher than that of an actuator without added carbon fiber). This advanced actuator holds significant promise for applications in fields such as soft machine grippers and artificial muscles, particularly in scenarios requiring high load capacity.

Use of AI tools declaration

The authors declare they have not used Artificial Intelligence (AI) tools in the creation of this article.

Acknowledgments

The work was supported by the National Natural Science Foundations of China (51975320 and U23A20627), the Beijing Natural Science Foundation (M22011) and the State Key Laboratory of Clean and Efficient Turbomachinery Power Equipment.

Author contributions

Haiyan Zhao and Jincong Chen conceived the study. Jincong Chen and Xiaodong Zhao completed the design, preparation, characterization and application experiments. All authors have given approval to the final version of the manuscript.

Conflict of interest

The authors declare no conflict of interest.

References

1. Liu H, Chu HX, Yuan HL, et al. (2024) Bioinspired multifunctional self-sensing actuated gradient hydrogel for soft-hard robot remote interaction. *Nano-Micro Lett* 16: 69. https://doi.org/10.1007/s40820-023-01287-z
2. Xu HF, Wu S, Liu Y, et al. (2024) 3D nanofabricated soft microrobots with super-compliant picoforce springs as onboard sensors and actuators. *Nat Nanotechnol* 19: 494–503. https://doi.org/10.1038/s41565-023-01567-0
3. Yang JY, Huang WT, Peng KL, et al. (2024) Versatile agar-zwitterion hybrid hydrogels for temperature self-sensing and electro-responsive actuation. *Adv Funct Mater* 34: 2313725. https://doi.org/10.1002/adfm.202313725
4. Wang HQ, Jiang H, Li YJ, et al. (2024) Electric-thermal dual-responsive HASEL actuator for solid-liquid bi-stabilized smart switching. *Adv Funct Mater* 34: 2409472. https://doi.org/10.1002/adfm.202409472
5. Zhu QL, Liu WX, Khoruzhenko O, et al. (2024) Closed twisted hydrogel ribbons with self-sustained motions under static light irradiation. *Adv Mater* 36: 2314152. https://doi.org/10.1002/adma.202314152
6. Skillin NP, Bauman GE, Kirkpatrick BE, et al. (2024) Photothermal actuation of thick 3D-printed liquid crystalline elastomer nanocomposites. *Adv Mater* 36: 2313745. https://doi.org/10.1002/adma.202313745
7. Gu M, Echtermeyer TJ (2024) A graphene-mica-based photo-thermal actuator for small-scale soft robots. *Small* 20: 2311001. https://doi.org/10.1002/smll.202311001
8. Tian XW, Guo YS, Zhang JQ, et al. (2024) Fiber actuators based on reversible thermal responsive liquid crystal elastomer. *Small* 20: 2306952. https://doi.org/10.1002/smll.202306952

9. Zeng SF, Ye YJ, Zhou PD, et al. (2024) Programmable and reconfigurable humidity-driven actuators made with MXene ($Ti_3C_2T_x$)-cellulose nanofiber composites for biomimetic applications. *Nano Res* 17: 6619–6629. https://doi.org/10.1007/s12274-024-6542-4
10. Weng X, Weng ZW, Qin M, et al. (2024) Bioinspired moisture-driven soft actuators based on MXene/aramid nanofiber nanocomposite films. *ACS Appl Nano Mater* 7: 5587–5597. https://doi.org/10.1021/acsanm.4c00420
11. Khalid MY, Arif ZU, Tariq A, et al. (2024) 3D printing of magneto-active smart materials for advanced actuators and soft robotics applications. *Eur Polym J* 205: 112718. https://doi.org/10.1016/j.eurpolymj.2023.112718
12. Wang B, Chen YR, Ye ZC, et al. (2024) Low-friction soft robots for targeted bacterial infection treatment in gastrointestinal tract. *Cyborg Bionic Syst* 5: 0138. https://doi.org/10.34133/cbsystems.0138
13. Yang Y, He ZG, Jiao PC, et al. (2024) Bioinspired soft robotics: How do we learn from creatures? *IEEE Rev Biomed Eng* 17: 153–165. https://doi.org/10.1109/RBME.2022.3210015
14. Zhang W, Jin K, Ren Z, et al. (2024) High-performance MXene/carbon nanotube electrochemical actuators for biomimetic soft robotic applications. *Adv Funct Mater* 34: 2408496. https://doi.org/10.1002/adfm.202408496
15. Nguyen V, Oh S, Mahato M, et al. (2024) Functionally antagonistic polyelectrolyte for electro-ionic soft actuator. *Nat Commun* 15: 435. https://doi.org/10.1038/s41467-024-44719-z
16. Nan MM, Guo KL, Jia T, et al. (2024) Novel acid-driven bioinspired self-resettable bilayer hydrogel actuator mimicking natural muscles. *ACS Appl Mater Interfaces* 16: 9224–9230. https://doi.org/10.1021/acsami.3c16500
17. Zhang L, Xing SC, Yin HF, et al. (2024) Skin-inspired, sensory robots for electronic implants. *Nat Commun* 15: 4777. https://doi.org/10.1038/s41467-024-48903-z
18. Kim H, Na H, Noh S, et al. (2024) Inherently integrated microfiber-based flexible proprioceptive sensor for feedback-controlled soft actuators. *npj Flex Electron* 8: 15. https://doi.org/10.1038/s41528-024-00302-6
19. Park J, Lee Y, Cho S, et al. (2024) Soft sensors and actuators for wearable human-machine interfaces. *Chem Rev* 124: 1464–1534. https://doi.org/10.1021/acs.chemrev.3c00356
20. Che ZY, Wan X, Xu J, et al. (2024) Speaking without vocal folds using a machine-learning-assisted wearable sensing-actuation system. *Nat Commun* 15: 1873. https://doi.org/10.1038/s41467-024-45915-7
21. Jin WY, Pei JY, Xie P, et al. (2023) Machine learning-based prediction of mechanical properties and performance of nickel-graphene nanocomposites using molecular dynamics simulation data. *ACS Appl Nano Mater* 6: 12190–12199. https://doi.org/10.1021/acsanm.3c01919
22. Jiao ZD, Hu ZH, Shi YH, et al. (2024) Reprogrammable, intelligent soft origami LEGO coupling actuation, computation, and sensing. *The Innovation* 5: 100549. https://doi.org/10.1016/j.xinn.2023.100549
23. Ma JN, Ma B, Wang ZX, et al. (2024) Multiresponsive MXene actuators with asymmetric quantum-confined superfluidic structures. *Adv Funct Mater* 34: 2308317. https://doi.org/10.1002/adfm.202308317
24. Li XL, Han DD, Zhang YC, et al. (2025) Direct laser scribing of all-solid-state in-plane proton microsupercapacitors on ionic covalent organic framework films. *Adv Funct Mater* 2423854. https://doi.org/10.1002/adfm.202423854

25. Tian JT, Cao WH (2024) Reconfigurable flexible metasurfaces: from fundamentals towards biomedical applications. *PhotoniX* 5: 2. https://doi.org/10.1186/s43074-023-00116-1
26. Sun ZW, Dang C, Zhang HM, et al. (2024) Lignin powered versatile bioelastomer: A universal medium for smart photothermal conversion. *Adv Funct Mater* 34: 2405130. https://doi.org/10.1002/adfm.202405130
27. Zhan LX, Chen SH, Xin YY, et al. (2024) Dual-responsive MXene-functionalized wool yarn artificial muscles. *Adv Sci* 11: 2402196. https://doi.org/10.1002/advs.202402196
28. Guo KX, Yang XH, Zhou C, et al. (2024) Self-regulated reversal deformation and locomotion of structurally homogenous hydrogels subjected to constant light illumination. *Nat Commun* 15: 1694. https://doi.org/10.1038/s41467-024-46100-6
29. López-Díaz A, Vázquez AS, Vázquez E (2024) Hydrogels in soft robotics: Past, present, and future. *ACS Nano* 18: 20817–20826. https://doi.org/10.1021/acsnano.3c12200
30. Zhou K, Sun RJ, Wojciechowski JP, et al. (2024) 4D multimaterial printing of soft actuators with spatial and temporal control. *Adv Mater* 36: 2312135. https://doi.org/10.1002/adma.202312135
31. Lu YW, Wu YM, Wu JL, et al. (2024) Electro-induced two-way shape memory thermoplastic polyamide elastomer/carbon nanotubes composites. *J Mater Res Technol* 29: 2062–2071. https://doi.org/10.1016/j.jmrt.2024.01.258
32. Iravani S, Varma RS (2024) MXenes for bioinspired soft actuators: Advancements in angle-independent structural colors and beyond. *Nano-Micro Lett* 16: 142. https://doi.org/10.1007/s40820-024-01367-8
33. Yang ZQ, Wang YT, Lan LD, et al. (2024) Bioinspired H-bonding connected gradient nanostructure actuators based on cellulose nanofibrils and graphene. *Small* 20: 2401580. https://doi.org/10.1002/smll.202401580
34. Chen JC, Cao YT, Pei JY, et al. (2023) Multifunctional actuator based on graphene/PDMS composite materials with shape programmable configuration and high photothermal conversion capability. *ACS Appl Mater Interfaces* 15: 31917–31926. https://doi.org/10.1021/acsami.3c06041
35. Lin S, Ma SQ, Chen KZ, et al. (2024) A humidity-driven film with fast response and continuous rolling locomotion. *Chem Eng J* 495: 153294. https://doi.org/10.1016/j.cej.2024.153294
36. Yu J, Xu ZP, Wan Q, et al. (2024) Ultrafast bi-directional bending moisture-responsive soft actuators through superfine silk rod modified bio-mimicking hierarchical layered structure. *Small* 20: 2309364. https://doi.org/10.1002/smll.202309364
37. Wang J, Zhou H, Fan YY, et al. (2024) Adaptive nanotube networks enabling omnidirectionally deformable electro-driven liquid crystal elastomers towards artificial muscles. *Mater Horiz* 11: 1877–1888. https://doi.org/10.1039/D4MH00107A
38. Wei J, Ma C, Zhang TT, et al. (2024) High-performance cellulose nanofibers-based actuators with multi-stimulus responses and energy storage. *Chem Eng J* 490: 151393. https://doi.org/10.1016/j.cej.2024.151393
39. Yang MJ, Yuan ZK, Liu J, et al. (2019) Photoresponsive actuators built from carbon-based soft materials. *Adv Opt Mater* 7: 1900069. https://doi.org/10.1002/adom.201900069
40. Wang M, Zhou L, Deng WY, et al. (2022) Ultrafast response and programmable locomotion of liquid/vapor/light-driven soft multifunctional actuators. *ACS Nano* 16: 2672–2681. https://doi.org/10.1021/acsnano.1c09477

41. Chathuranga H, Marriam I, Chen S, et al. (2022) Multistimulus-responsive graphene oxide/Fe_3O_4/starch soft actuators. *ACS Appl Mater Interfaces* 14: 16772–16779. https://doi.org/10.1021/acsami.2c03486
42. Sales FCP, Ariati RM, Noronha VT, et al. (2022) Mechanical characterization of PDMS with different mixing ratios. *Proc Struct Integr* 37: 383–388. https://doi.org/10.1016/j.prostr.2022.01.099
43. Kinloch IA, Suhr J, Lou J, et al. (2018) Composites with carbon nanotubes and graphene: An outlook. *Science* 362: 547–553. https://doi.org/10.1126/science.aat7439
44. Tang ZH, Gao ZW, Jia SH, et al. (2017) Graphene-based polymer bilayers with superior light-driven properties for remote construction of 3D structures. *Adv Sci* 4: 1600437. https://doi.org/10.1002/advs.201600437
45. Li B, Dong S, Wu X, et al. (2017) Anisotropic thermal property of magnetically oriented carbon nanotube/graphene polymer composites. *Compos Sci Technol* 147: 52–61. https://doi.org/10.1016/j.compscitech.2017.05.006

Supplementary

1. Details in the manufacturing process of actuators; details of finite element calculation (Word)
2. NIR photoresponsive properties of carbon fiber reinforced actuators (MP4)